Graph Fractional-Order Total Variation EEG Source Localization

Jing Qin

Department of Mathematical Sciences
Montana State University

Joint work with Ying Li, Tianyu Wu, Wotao Yin
Wentai Liu and Stanley Osher

June 22, 2017

Outline

- Introduction
- s-SMOOTH
- gFOTV EEG Reconstruction Model
- Accelerated Algorithms
- Conclusions and Future Work

EEG

Electroencephalography (EEG) is a non-invasive test for detecting epilepsy, brain tumor, trauma and congenital defects (sources).

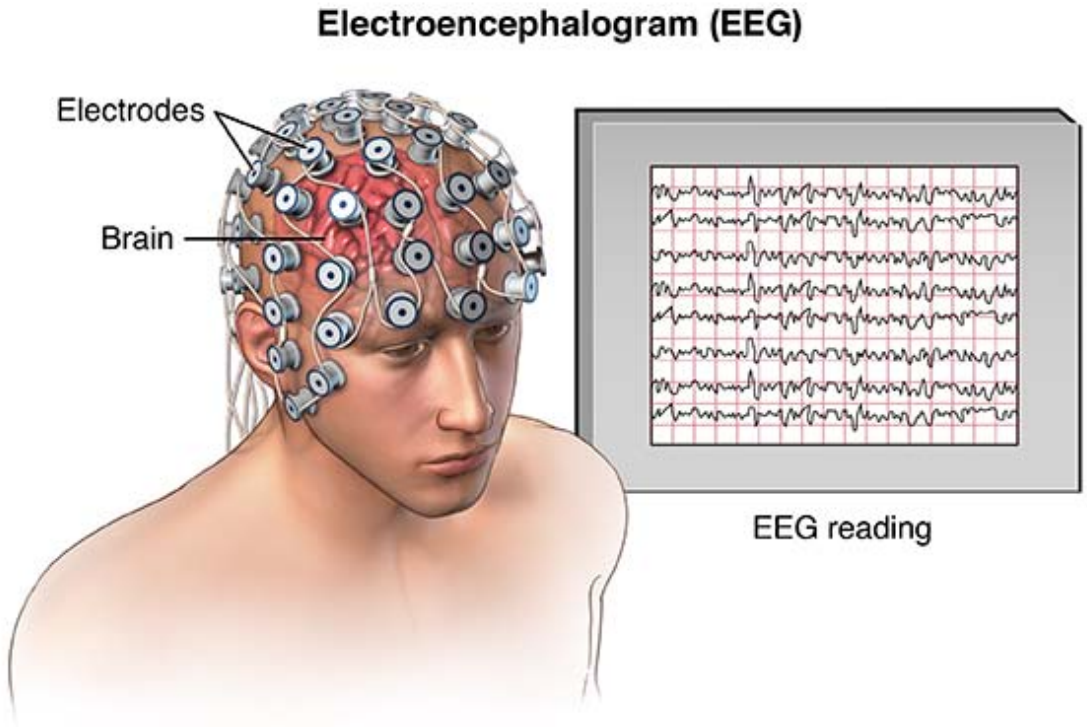

EEG Forward and Inverse Problems

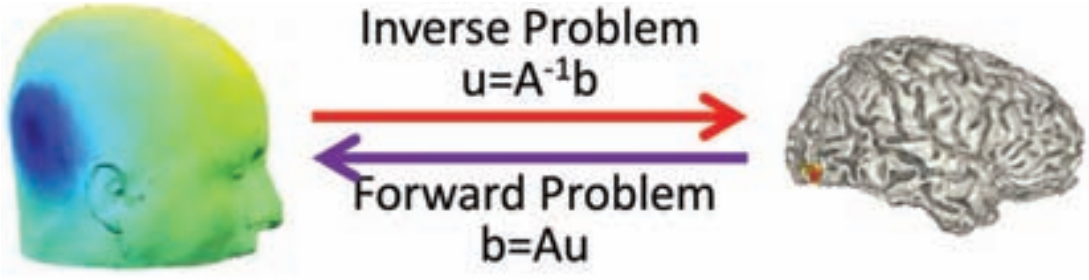

- **EEG forward problem**: given electrical sources, calculate the potentials at the electrodes. Under quasi-static conditions $\nabla \times \mathbf{E} = \mathbf{0}$ in Maxell's equation, Helmholtz decomposition yields Poisson's equation

$$\nabla \cdot (\sigma \nabla V) = -I_m$$

  where V is potential field, σ is conductivity and I_m is source current density in a volume conductor model.

- **EEG inverse problem**: find brain sources which are responsible for the measured potentials at the EEG electrodes (also called EEG source localization).

EEG Source Localization

$$b = Au + n$$

- $b \in \mathbb{R}^N$ - electrical potential measured on the scalp
- $u \in \mathbb{R}^M$ - neural current density distributed at each dipole location ($N \ll M$, e.g., $N = 324$, $M = 16384$)
- $A \in \mathbb{R}^{N \times M}$ - lead field matrix where $A_{i,j}$ is the electrical potential measured by the ith electrode due to an unit dipole source at the jth voxel (A is obtained by solving the forward problem)
- n - noise including background neural noise and electrode noise

Challenges

- Difficult to locate the source peak with high accuracy.
- Sophisticated geometry of the cortical surface.
- Large amount of data, e.g., 16384 voxels in our experiment.
- Noise, including background neural noise, electronic noise and electrode noise.

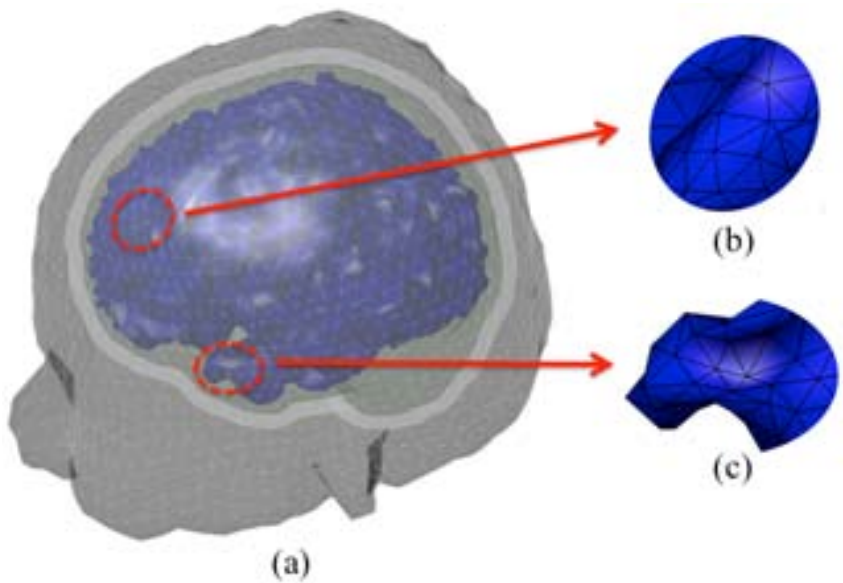

Figure: (a) Realistic head model constructed from the MRI of the subject. From outside in are: scalp (grey), skull (white), brain (green), source model (blue). (b)(c) Close-up of the source model showing the triangular mesh.

Previous Work

- Minimum Norm Estimate (MNE) [Hämäläinen et al. ’93]
- Low Resolution Electrical TomograAphy (LORETA) [Rascual-Marqui et al. ’94]
- FOCal Under-determined System Solution (FOCUSS) [Gorodnitsky et al. ’95]
- Quadratic regularization and spatial regularization (S-MAP) using dipole intensity gradients [Baillet-Garnero ’97]
- Minimum Current Estimate (MCE) [Hämäläinen ’99]
- standardized Low Resolution brain Electromagnetic TomograAphy (sLORETA) [Rascual-Marqui ’02]
- total variation (TV) based methods [Ding ’09, Becker et al. ’14]

Sparsity and SMOOthness enhanced brain TomograpHy (s-SMOOTH)

Motivation

Illustration of piecewise polynomial current densities in 3D view and sideview:

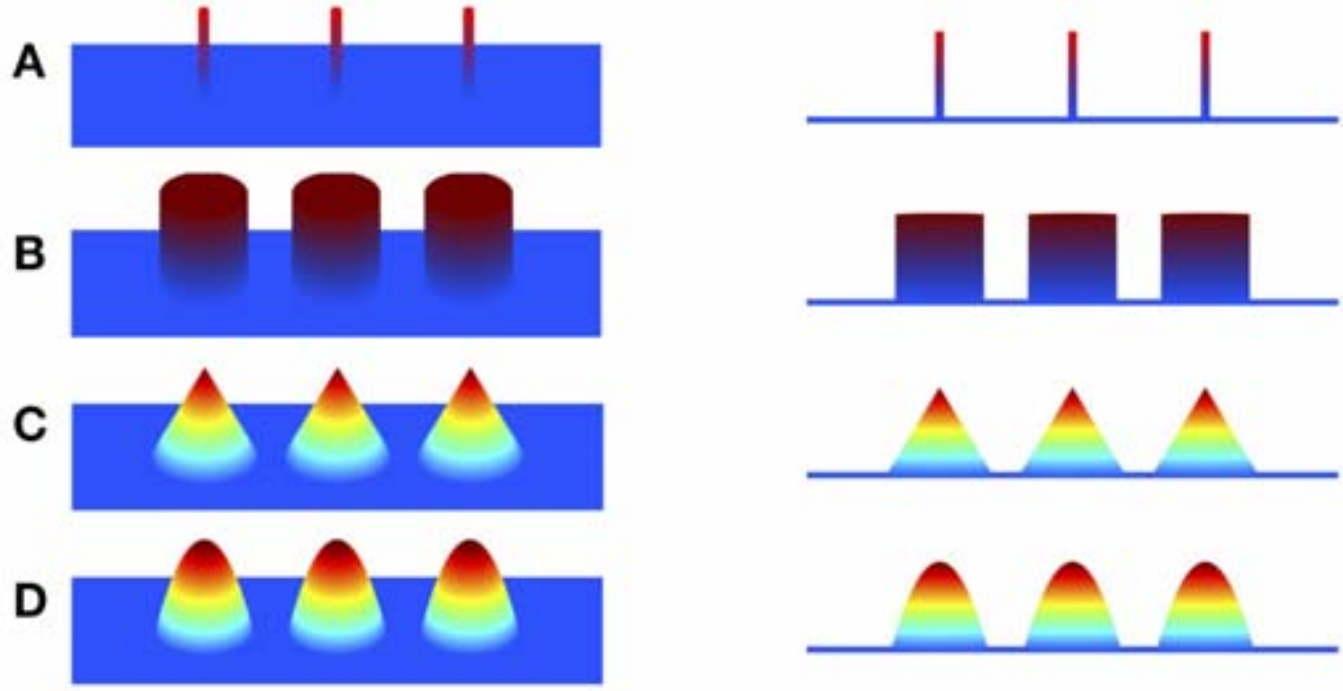

(A–D): Impulse(sparse in itself), piecewise constant (sparse in first spatial derivative), piecewise linear(sparse in second derivative), piecewise quadratic(sparse in third derivative).

Higher Order Smoothness

- Total variation (TV)

$$\mathrm{TV}(u) = \sup \left\{ \int_\Omega u \operatorname{div} v \, dx \,\middle|\, v \in C_c^2(\Omega, \mathbb{R}), \|v\|_\infty \leq 1 \right\}.$$

- Total Generalized Variation (TGV) of order k with positive weights $\alpha = (\alpha_0, \cdots, \alpha_{k-1})$ (Bredies et al. '10) is defined as:

$$\mathrm{TGV}_\alpha^k(u) = \sup \left\{ \int_\Omega u \operatorname{div}^k v \, dx \,\middle|\, v \in C_c^k(\Omega, \mathrm{Sym}^k(\mathbb{R}^d)), \right.$$
$$\left. \|\operatorname{div}^l v\|_\infty \leq \alpha_l, \; l = 0, \cdots, k-1 \right\},$$

where $\mathrm{Sym}^k(\mathbb{R}^d)$ is the space of *symmetric tensors* on $\mathbb{R}^d$.

Reduce Staircasing Effects

noisy input TV TGV

Figure: Image smoothing results of TV and TGV. Courtesy of Bredies et al. ’10.

Reformulation of TGV

Let $U = C_c^2(\Omega, \mathbb{R})$, $V = C_c^2(\Omega, \mathbb{R}^2)$ and $W = C_c^2(\Omega, \mathrm{Sym}^2(\mathbb{R}^2))$. The second-order TGV with $\alpha = (\alpha_0, \alpha_1)$

$$\begin{aligned}\mathrm{TGV}_\alpha^2(u) &= \max\left\{\langle u, \operatorname{div}^2 w\rangle \,\middle|\, w \in W,\ \|w\|_\infty \le \alpha_0,\ \|\operatorname{div} w\|_\infty \le \alpha_1\right\} \\ &= \min_{p \in V} \max_{\substack{v \in V, \|v\|_\infty \le \alpha_1 \\ w \in W, \|w\|_\infty \le \alpha_0}} \langle \nabla u - p, v\rangle + \langle \mathcal{E}(p), w\rangle\end{aligned}$$

where $\langle u, \operatorname{div} v\rangle = -\langle \nabla u, v\rangle$, $\langle p, \operatorname{div} w\rangle = -\langle \mathcal{E}(p), w\rangle$ and

$$\nabla u = [\partial_x u, \partial_y u]^T, \quad \mathcal{E}(p) = \begin{bmatrix} \partial_x p_1 & \frac{1}{2}(\partial_y p_1 + \partial_x p_2) \\ \frac{1}{2}(\partial_y p_1 + \partial_x p_2) & \partial_y p_2 \end{bmatrix}.$$

Second-order TGV can be written as [Guo-Q.-Yin '14]

$$\mathrm{TGV}_\alpha^2(u) = \min_{p \in V} \alpha_1 \|\nabla u - p\|_1 + \alpha_0 \|\mathcal{E}(p)\|_1$$

vTGV

Voxel-based Total Generalized Variation (vTGV) on a triangular mesh:

$$\mathrm{vTGV}^2_\alpha(u) = \min_p \alpha_1 \|Du - p\|_1 + \alpha_2 \|Ep\|_1,$$

where

$$D_{i,j} = \begin{cases} 1, & \text{if } j = l; \\ -1, & \text{if } j \in \{k_{l,1}, k_{l,2}, k_{l,3}\}; \\ 0, & \text{otherwise.} \end{cases}$$

$$E = \frac{1}{2}(\widehat{D} + \widehat{D}^T), \quad \text{where} \quad \widehat{D} = \begin{bmatrix} D & D & D \end{bmatrix}$$

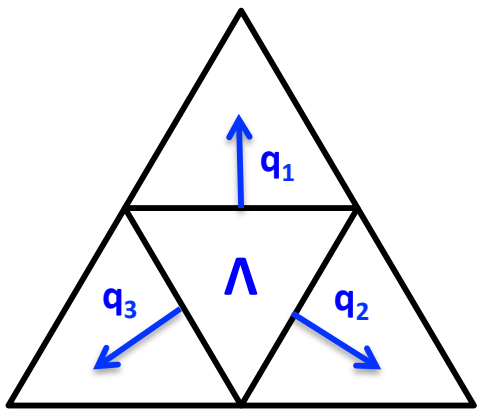

Sparsity Enhanced Regularization

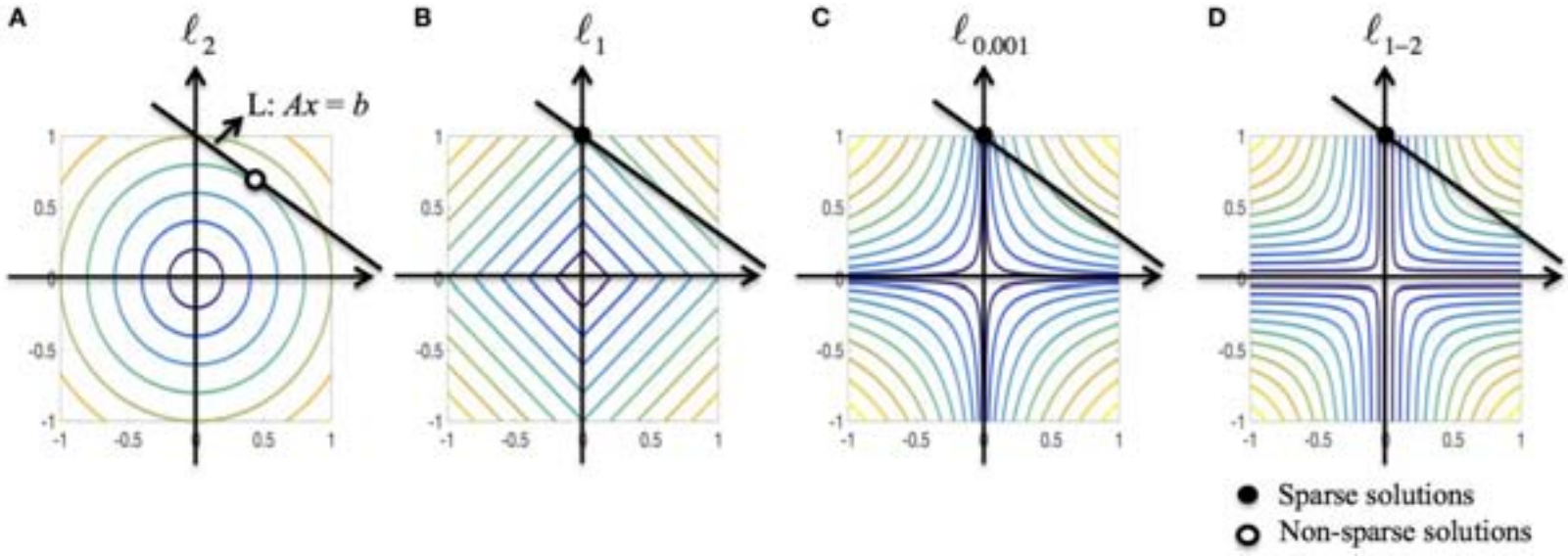

ℓ_2, ℓ_1, $\ell_{0.001}$ (used to approximate ℓ_0) and $\ell_{1-2} := \ell_1 - \beta\ell_2$ when $\beta = 1$. The black line corresponds to the linear constraint, the solid dot specifies the sparse solution and the circular dot specifies the non-sparse solution.

s-SMOOTH

s-SMOOTH EEG brain image reconstruction method
[Li-Q.-Liu-Osher '16]

$$\min_u \tfrac{1}{2}\|Au-b\|_2^2 + \mathrm{TGV}_\alpha^2(u) + \lambda(\|u\|_1 - \beta\|u\|_2)$$

Next we apply the difference of convex function algorithm (DCA)

$$\begin{cases} q \leftarrow u/\|u\|_2, \\ (u,p) \leftarrow \operatorname{argmin}_{u,p} \dfrac{1}{2}\|Au-b\|_2^2 + \alpha_1\|Du-p\|_1 + \alpha_2\|Ep\|_1 \\ \qquad\qquad + \alpha_3(\|u\|_1 - \beta\langle u,q\rangle). \end{cases} \tag{1}$$

Here the second subproblem is first rewritten by change of variables and then solved by ADMM:

$$\min_{u,p,x,y,z} \frac{1}{2}\|Au-b\|_2^2 + \alpha_1\|x\|_1 + \alpha_2\|y\|_1 + \alpha_3(\|z\|_1 - \beta\langle z,q\rangle)$$

$$\text{subject to} \quad x = Du-p,\ y = Ep,\ z = u.$$

Result

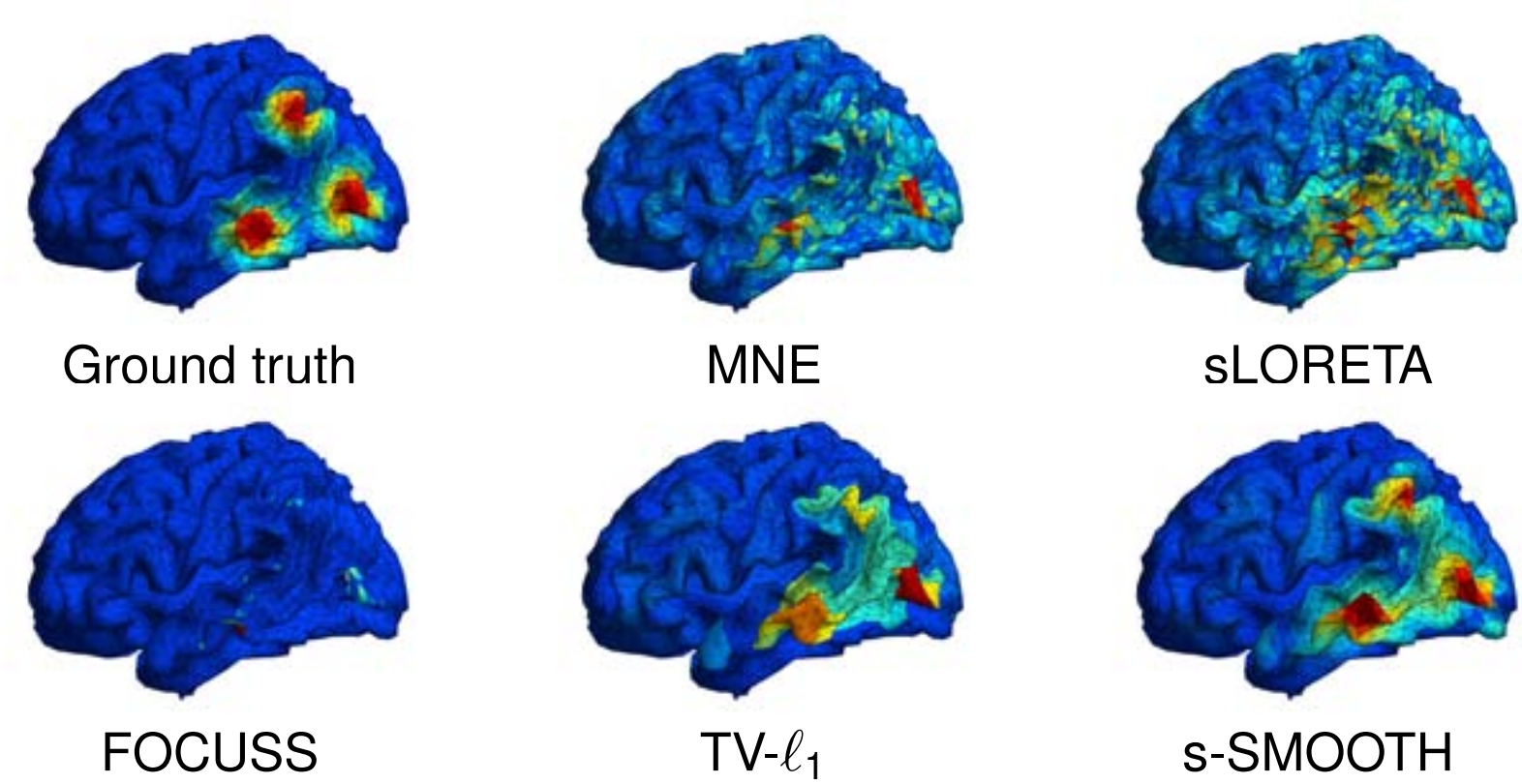

Figure: Source localization results of various methods on synthetic data with multiple sources. The color scale gradation goes from blue being the minimum to red being the maximum.

Cons: parameter tuning and computational burden.

Graph Fractional-Order Total Variation EEG Reconstruction

Fractional-order Derivatives I

Given $\alpha \in \mathbb{R}^+$ such that $0 \leq n-1 < \alpha < n$ with $n \in \mathbb{N}$.

- Riemann-Liouville (RL)

$$D^{\alpha}_{[a,x]} f(x) = \frac{1}{\Gamma(n-\alpha)} \left(\frac{d}{dx}\right)^n \int_a^x \frac{f(\tau)}{(x-\tau)^{\alpha-n+1}} d\tau$$

$$D^{\alpha}_{[x,b]} f(x) = \frac{(-1)^n}{\Gamma(n-\alpha)} \left(\frac{d}{dx}\right)^n \int_x^b \frac{f(\tau)}{(\tau-x)^{\alpha-n+1}} d\tau$$

$$D^{\alpha}_{[a,b]} f(x) = \frac{1}{2}\left(D^{\alpha}_{[a,x]} f(x) + (-1)^n D^{\alpha}_{[x,b]} f(x)\right)$$

- Caputo

$${}^{C}D^{\alpha}_{[a,x]} f(x) = \frac{1}{n-\alpha} \int_a^x \frac{f^{(n)}(\tau)}{(x-\tau)^{\alpha-n+1}} d\tau$$

$${}^{C}D^{\alpha}_{[x,b]} f(x) = \frac{(-1)^n}{\Gamma(n-\alpha)} \int_x^b \frac{f^{(n)}(\tau)}{(\tau-x)^{(\alpha-n+1)}} d\tau$$

$${}^{C}D^{\alpha}_{[a,b]} f(x) = \frac{1}{2}\left({}^{C}D^{\alpha}_{[a,x]} f(x) + (-1)^{n\,C} D^{\alpha}_{[x,b]} f(x)\right)$$

Fractional-order Derivatives II

- Grünwald-Letnikov (GL)

$$ {}^{G}D^{\alpha}_{[a,x]} f(x) = \lim_{h\to 0} \frac{1}{h^{\alpha}} \sum_{j=0}^{[(x-a)/h]} (-1)^j \binom{\alpha}{j} f(x-jh). $$

Theorem (Singularity)

Assume that $D^{\alpha}_{[a,x]}$ is one of the above three fractional-order derivatives. For any noninteger $\alpha > 0$ and $x > a$, then

$$ \begin{aligned} D^{\alpha}_{[0,x]}(x-2\tau)(x-\tau)^{\alpha} &= 0, \quad && 0 < \alpha < 1 \\ D^{\alpha}_{[a,x]}(x-\tau)^{\alpha-1} &= 0, && \alpha > 1 \\ {}^{C}D^{\alpha}_{[a,x]}(x-\tau)^{n-1} &= 0, && \alpha > 0. \end{aligned} $$

Remark $D^{\alpha}_{[0,x]} f(x) = 0$ if $f(x) = x^{\alpha-1}$ or $x^{\alpha-2}$ for $\alpha \in (1,2)$, e.g., $f(x) = x^{0.6}$ or $x^{-0.4}$ when $\alpha = 1.6$.

Fractional-order Total Variation

$$TV_\alpha(u) = \|\nabla^\alpha u\|_1 = \sum_{i,j=1}^{N} \left(|(D_x^\alpha u)_{i,j}| + |(D_y^\alpha u)_{i,j}| \right),$$

where $\alpha \in (1, 2)$. Here the fractional derivative is based on the Grüwald-Letnikov derivative definition ($h = 1$)

$$(D_x^\alpha u)_{i,j} = \sum_{k=0}^{K} w_\alpha(k) u(i-k, j), \; (D_y^\alpha u)_{i,j} = \sum_{k=0}^{K} w_\alpha(k) u(i, j-k),$$

where the coefficients are

$$w_\alpha(k) = (-1)^k \frac{\Gamma(\alpha+1)}{k!\Gamma(\alpha-k+1)}.$$

Remark $w_\alpha(0) = 1$ and $w_\alpha(1) = -\alpha$.

Properties

- The adjoint operator of D_α is defined by

$$(D_x^{\alpha *} u)_{i,j} = \sum_{k=0}^{K} w_\alpha(k) u(i+k, j),$$

$$(D_y^{\alpha *} u)_{i,j} = \sum_{k=0}^{K} w_\alpha(k) u(i, j+k).$$

- If $\alpha = 1$, then $w_1(0) = 1$, $w_1(1) = -1$, $w_1(k) = 0$ for $k > 1$.
- If $\alpha = 2$, then $w_2(0) = 1$, $w_2(1) = -2$, $w_2(2) = 1$ and $w_2(k) = 0$ for $k > 2$.
- If $\alpha \in (1, 2)$, then $w_\alpha(k) \to 0$ as $k \to \infty$. If $\alpha \to 2$, $w_\alpha(k)$ decays faster. If $\alpha \to 1$, $w_\alpha(k)$ decays slower.

Graph Fractional-order TV

Given a path $p = (v_{i=m_0}, v_{m_1}, \ldots, v_{m_K})$ where the shortest distance between the nodes v_{m_0} and v_{m_j} is j nodes, the fractional-order derivative along the path p is defined as

$$(D_p^\alpha u)_i := D_p^\alpha u(v_i) = \sum_{v \in p} w_\alpha(d(v_i, v))u(v) = \sum_{j=0}^{K} w_\alpha(j)u(v_{m_j}).$$

The graph fractional-order TV of u is defined as follows:

$$TV_\alpha(u) = \|D_\alpha u\|_1 = \sum_{i=1}^{M} \sum_{p \in \mathcal{P}(i;K)} |(D_p^\alpha u)_i|,$$

where $\mathcal{P}(i; K)$ is the set of all paths starting from the ith node with length K nodes.

Illustration

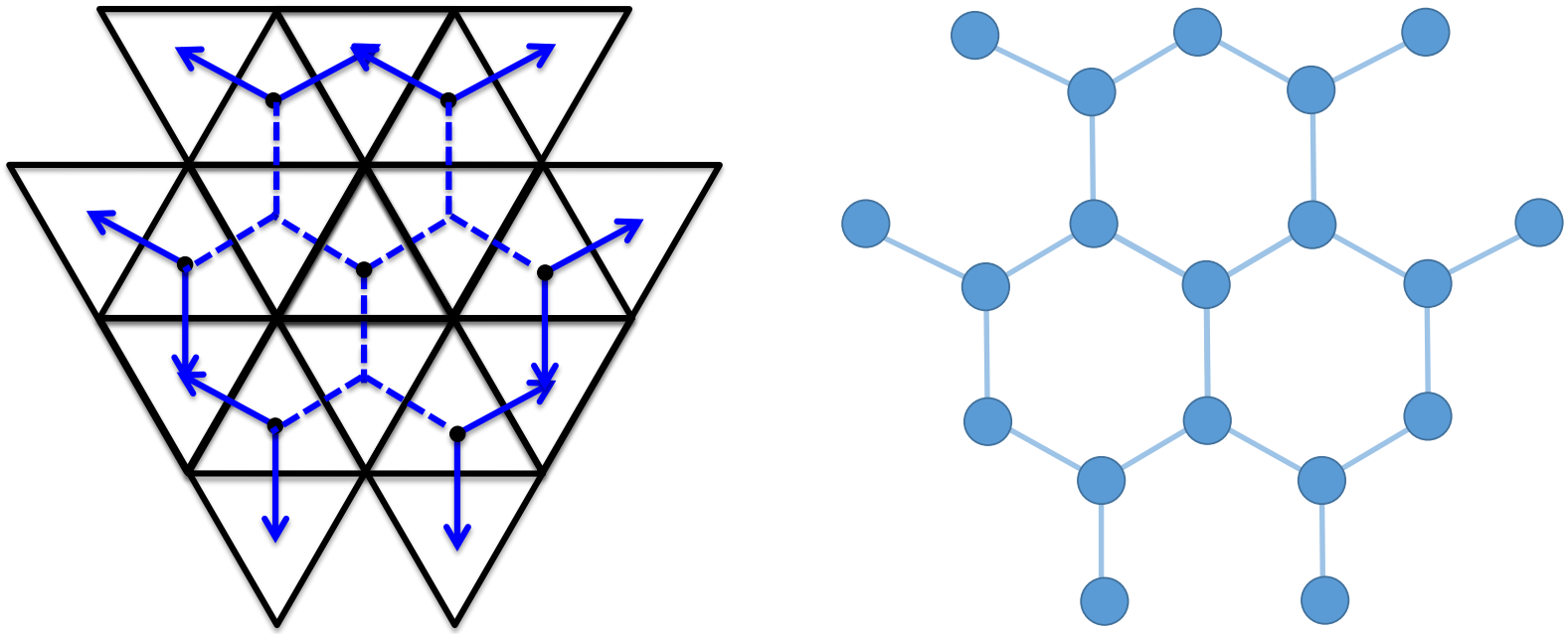

Figure: Every triangle is treated as a node of the graph. From left to right: four-level triangular mesh, four-level nodes.

The shortest path between each node pair can be calculated by the breadth-first search (BFS) algorithm.

Proposed Method

gFOTV EEG source reconstruction[Li-Q.-Liu-Osher '16]

$$\min_u \left\{ \frac{1}{2}\|Au - b\|_2^2 + \lambda TV_\alpha(u) \right\}. \tag{2}$$

Rewrite it as

$$\min_{u,v} \left\{ \frac{1}{2}\|Au - b\|_2^2 + \lambda\|v\|_1 \right\} \quad \text{subject to} \quad D_\alpha u = v.$$

where $D_\alpha \in \mathbb{R}^{L\times N}$ with $L = 3N \cdot 2^{K-1}$. Then the ADMM/split Bregman yields

$$\begin{cases} v = \text{shrink}(D_\alpha u + \tilde{v}, \lambda/\rho) \\ u = \underset{u}{\text{argmin}} \left\{ \frac{1}{2}\|Au - b\|_2^2 + \frac{\rho}{2}\|D_\alpha u - v + \tilde{v}\|_2^2 \right\} \\ \quad = (A^TA + \rho D_\alpha^T D_\alpha)^{-1}\left(A^Tb + \rho D_\alpha^T(v - \tilde{v})\right) \\ \tilde{v} \leftarrow \tilde{v} + \gamma(D_\alpha u - v), \quad \gamma \in (0, (\sqrt{5}+1)/2). \end{cases} \tag{3}$$

Qualitative Comparison

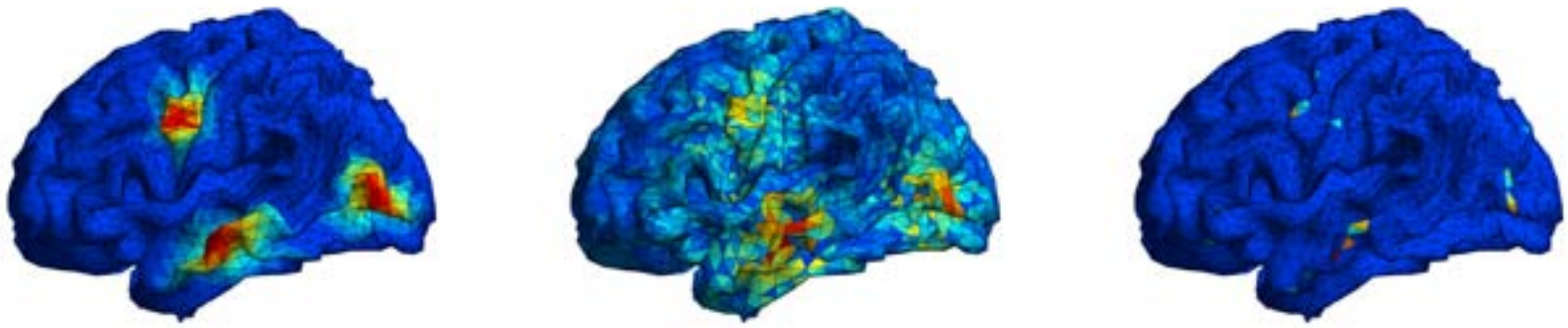

Ground truth | sLORETA | MCE

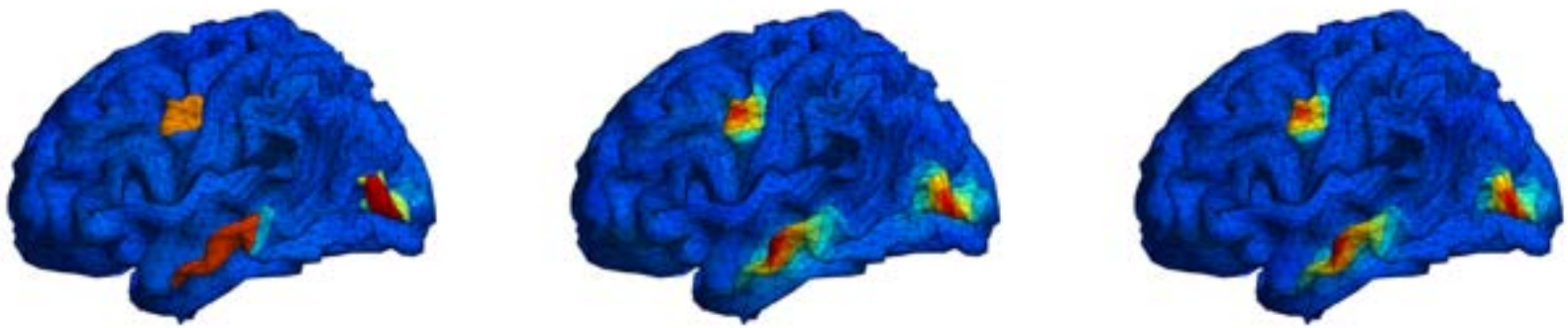

TV | $gFOTV_2$ | $gFOTV_{1.6}$

Figure: Source localization results of various methods on synthetic data with three sources. The color scale gradation goes from blue being the minimum to red being the maximum.

Quantitative Criteria

- Total Reconstruction Error (TRE)

$$TRE = \|\hat{u} - u\|_2 / \|u\|_2$$

where u and $\hat{u}$ are the ground truth and the reconstructed source respectively.

- Averaged Localization Error (ALE)

$$ALE = \sum_k LE_k / K,\ LE_k = \{d_{ki} | i = \underset{i' \in I_k}{\operatorname{argmin}} \|u_{i'}\|_2\}.$$

where d_{ki} is the distance between the ith voxel to the peak of the kth true source, and I_k is a set of the voxel indices that are closest to the kth source peak.

- Degree of Focalization (DF)

$$DF = \|\hat{u}_S\|_2^2 / \|u_S\|_2^2$$

where u_S is u restricted on the original patch area S.

Quantitative Comparison

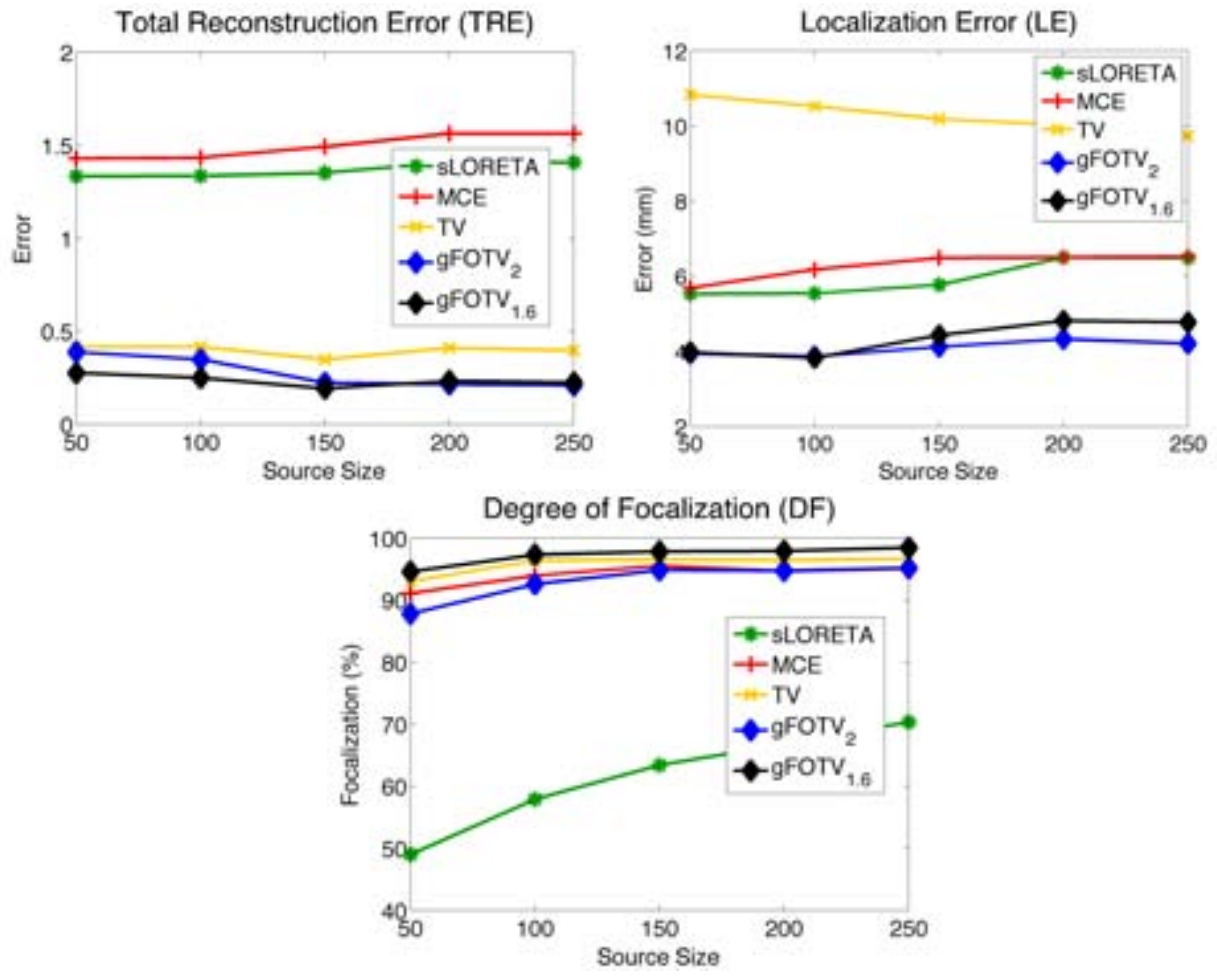

Figure: Quantitative comparisons of various methods with different source sizes (average of 50 noise configurations).

Accelerated Algorithms

Application of Chambolle-Pock Algorithm

Apply the Chambolle-Pock algorithm with diagonal preconditioning [Pock-Chambolle '11] to solve (2)

$$\begin{cases} u^{k+1} = u^k - \Sigma(D_\alpha^T s^k + A^T t^k) \\ s^{k+1} = \mathrm{proj}_{\|\cdot\|_\infty \le \lambda}(s^k + \Gamma_1 D_\alpha(u^k - 2\Sigma(D_\alpha^T s^k + A^T t^k))) \\ t^{k+1} = (I + \Gamma_2)^{-1}(t^k - \Gamma_2 b + \Gamma_2 A^T(2u^{k+1} - u^k)). \end{cases} \quad (4)$$

Here $\Sigma, \Gamma_1, \Gamma_2$ are diagonal matrices controlling the step sizes, which are defined by

$$\begin{cases} \Sigma_{ii} = (\sum_{j=1}^{L} |(D_\alpha)_{ji}| + \sum_{j=1}^{M} |A_{ji}|)^{-1} \\ (\Gamma_1)_{ii} = (\sum_{j=1}^{N} |(D_\alpha)_{ij}|)^{-1} \\ (\Gamma_2)_{ii} = (\sum_{j=1}^{N} |A_{ij}|)^{-1}. \end{cases}$$

Coordinate Updating Scheme

Based on the technique in [Peng et al. '16], we first rewrite (4)

$$\begin{cases} u^{k+1} = u^k - \Sigma(D_\alpha^T s^k + A^T t^k) \\ s^{k+1} = \mathrm{proj}_{\|\cdot\|_\infty \le \lambda}(s^k + \Gamma_1 D_\alpha(u^k - 2\Sigma(D_\alpha^T s^k + A^T t^k))) \\ t^{k+1} = (I + \Gamma_2)^{-1}(t^k - \Gamma_2 b + \Gamma_2 A^T(u^k - 2\Sigma(D_\alpha^T s^k + A^T t^k))), \end{cases} \tag{5}$$

By letting $z^k = (u^k, s^k, t^k)^T$, (5) can be rewritten as

$$z^{k+1} = Tz^k.$$

Randomly update one coordinate of z, say $z_i^{k+1} = (Tz^k)_i$, and keep the rest coordinates unchanged, i.e., $z_j^{k+1} = z_j^k$ for $j \neq i$.

Proposed Algorithm

Algorithm 1: Async-parallel update

Input : $z^0 \in \mathbb{R}^{N+L+M}$, $K > 0$, $0 < \rho < 1$, $(q_1, \ldots, q_{N+L+M})$ where $q_i > 0$, $\sum_{i=1}^{N+L+M} q_i = 1$

Set the global iteration counter $k = 0$;

while $k < K$, *every agent asynchronously* **do**

- Select $1 \leq i_k \leq N + L + M$ with $\mathrm{Prob}(i_k = i) = q_i$;
- Compute $\hat{z}_{i_k}^{k+1}$ according to (5);
- Update $z_{i_k}^{k+1} = (1 - \rho) z_{i_k}^k + \rho \hat{z}_{i_k}^{k+1}$;
- Update the global counter $k \leftarrow k + 1$;

- it is *coordinate-friendly*
- it allows larger step sizes than its full update counterpart.
- all the step-size matrices $\Sigma, \Gamma_1, \Gamma_2$ are multiplied by a scaling factor $s \geq 1$, which empirically leads to faster convergence.

Experiment Setup

- compare Algorithm 1 with the ADMM-based algorithm [Li-Q.-Liu-Osher '16] and the CVX toolbox `http://cvxr.com/cvx/`. The toolbox has been used in the state-of-the-art EEG methods.
- We apply the fractional-order TV regularized model with $\alpha = 1.6$, which consistently yields superior performance compared to other related models in terms of accuracy.
- All numerical experiments are performed in a machine with an Intel® Xeon® CPU E5-2650 v4 @ 2.2GHz and 64GB RAM in double precision. The CPU has 12 physical cores and each core has 2 logical processors. Both ADMM and CVX are called in Matlab 2016a.

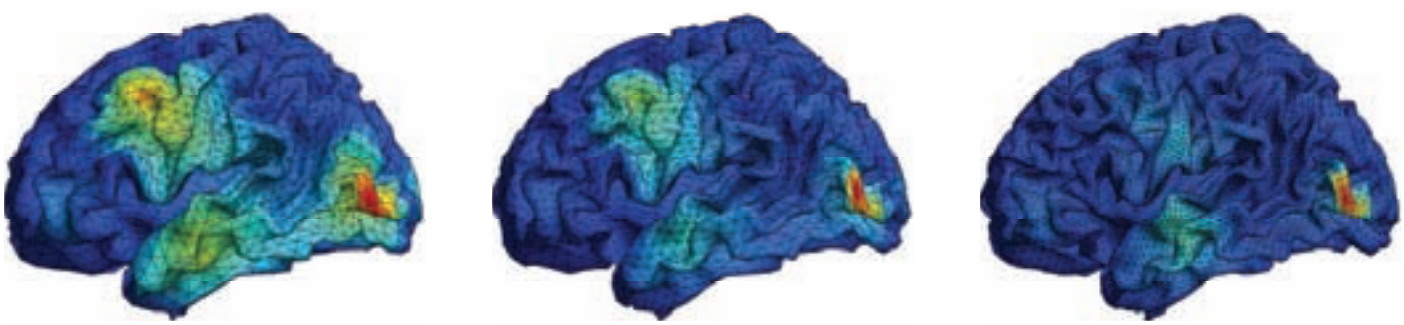

68 × 10240 | 68 × 16384 | 68 × 40960

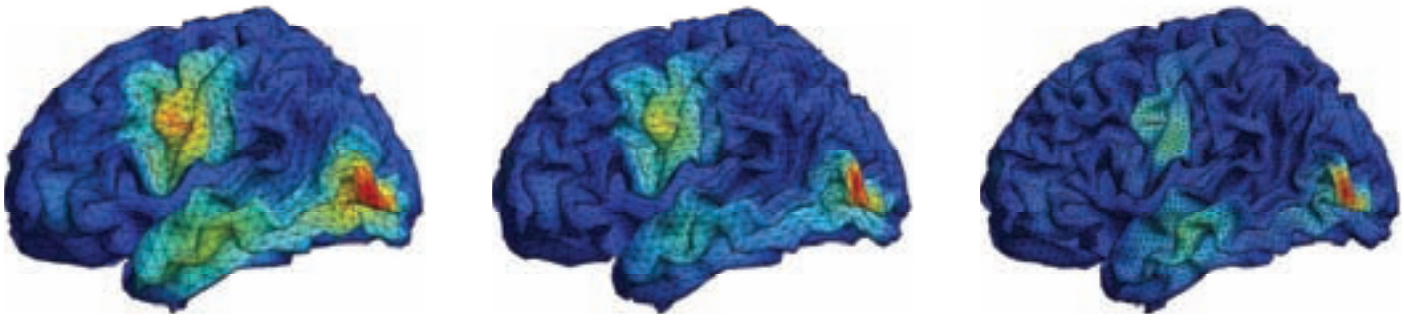

103 × 10240 | 103 × 16384 | 103 × 40960

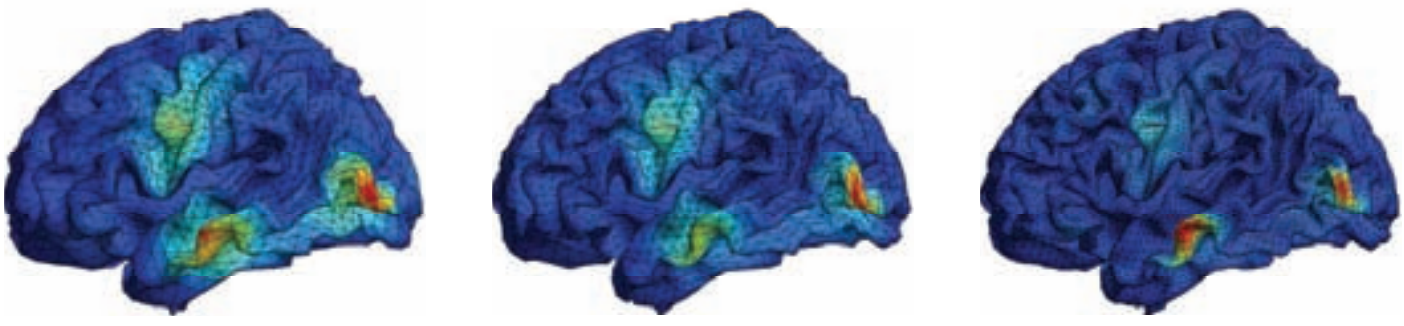

346 × 10240 | 346 × 16384 | 346 × 40960

Figure: Reconstructed images (No. of electrodes × No. of voxels).

Computation time comparison

Columns 3-6 list the computation times (in seconds) of single-threaded CVX, ADMM and the algorithm (1) with one thread and 16 threads, respectively.

M	N	CVX	ADMM	$p = 1$	$p = 16$
68	10240	52.78	67.36	40.30	4.90
68	16384	95.00	237.80	74.46	8.46
68	40960	311.71	2015.79	242.42	25.45
103	10240	62.37	64.21	33.00	3.84
103	16384	108.16	175.31	56.19	6.35
103	40960	393.23	1639.51	194.48	19.77
346	10240	370.63	51.02	45.14	5.21
346	16384	476.16	135.12	66.45	7.59
346	40960	2720.28	1200.10	177.15	19.70

Speedup Comparison

Define the speedup ratio as:

$$\frac{\text{running time using 1 thread}}{\text{running time using } p \text{ threads}},$$

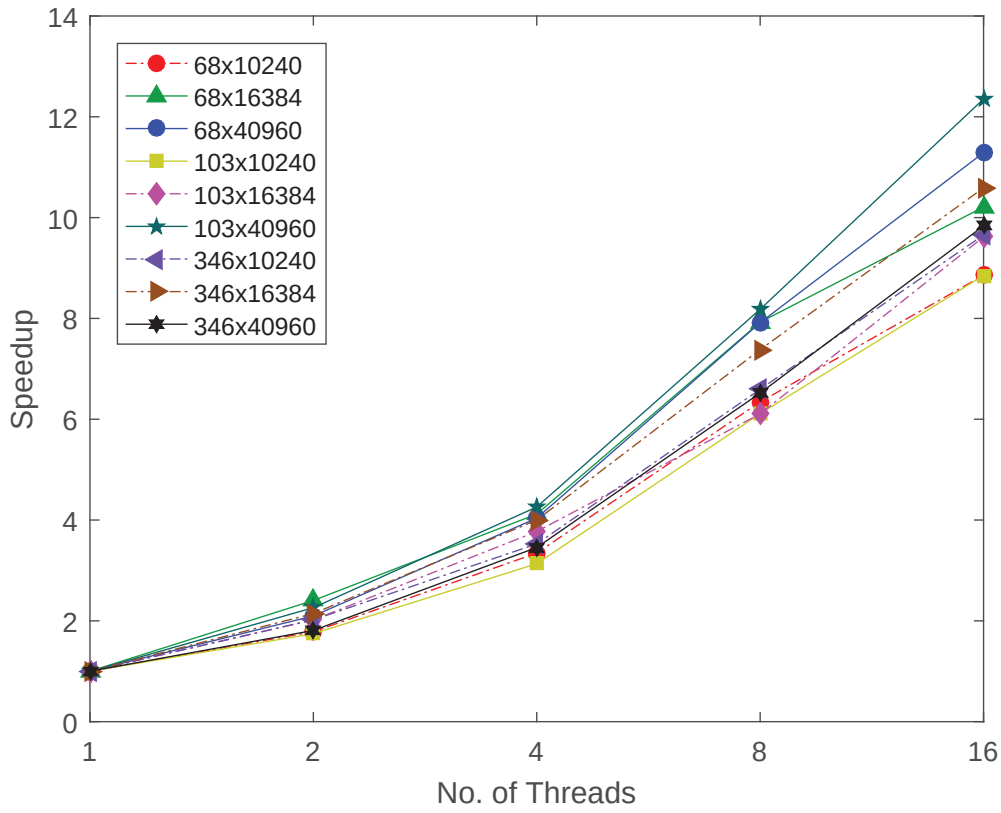

Conclusions and Future Work

Conclusions

- Both s-SMOOTH and gFOTV can preserve higher order smoothness.
- The proposed algorithms are parameter-friendly and converge fast with high accuracy.
- The accelerated algorithms using the asynchronous coordinate updating scheme and diagonal preconditioning are able to achieve real-time processing.

Future Work

- Extend this work to process EEG video.
- Consider geometry of cortex surface.
- Combine this framework into the dictionary learning based EEG signal classification.

References I

- M. Hämäläinen, R. Hari, R. J. Ilmoniemi, J. Knuutila, and O. V. Lounasmaa, “Magnetoencephalography–theory, instrumentation, and applications to noninvasive studies of the working human brain,” Reviews of modern Physics, 65(2):413, 1993.
- R. D. Pascual-Marqui, C. M. Michel, and D. Lehmann. ”Low resolution electromagnetic tomography: a new method for localizing electrical activity in the brain.” International Journal of psychophysiology 18.1: 49-65, 1994.
- I. F. Gorodnitsky, J. S. George, B. D. Rao, “Neuromagnetic source imaging with FOCUSS: a recursive weighted minimum norm algorithm,” Electroencephalography and Clinical Neurophysiology, 95(4): 231-251, 1995.
- S. Baillet, L. Garnero, “A Bayesian Approach to Introducing Anatomo-Functional Priors in the EEG/MEG Inverse Problem,” IEEE Transactions on Biomedical Engineering, 44(5): 374–385, 1997.
- K. Uutela, M. Hämäläinen, and E. Somersalo, “Visualization of magnetoencephalographic data using minimum current estimates,” NeuroImage, 10(2):173–180, 1999.
- R. D. Pascual-Marqui, “Standardized low-resolution brain electromagnetic tomography (sLORETA): technical details,” Methods Find Exp Clin Pharmacol, 24(Suppl D): 5–12, 2002.
- L. Ding, “Reconstructing cortical current density by exploring sparseness in the transform domain,” Physics in Medicine and Biology, 54(9):2683, 2009.

References II


H. Becker, L. Albera, P. Comon, R. Gribonval, and I. Merlet. “Fast, variation-based methods for the analysis of extended brain sources,” In *Signal Processing Conference (EUSIPCO), 2014 Proceedings of the 22nd European*, IEEE, 2014, pp. 41-45.


R. Oostenveld, D. F. Stegeman, P. Praamstra, and A. van Oosterom, “Brain symmetry and topographic analysis of lateralized event-related potentials,” Clinical neurophysiology, 114(7):1194–1202, 2003.


W. Guo, J. Qin and W. Yin. *A New Detail-preserving Regularization Scheme*, SIAM J. Imaging Sci. 7-2:1309-1334, 2014.


Y. Li, J. Qin, Y. Hsin, W. Liu and S. Osher, “s-SMOOTH: Sparsity and Smoothness Enhanced EEG Brain Tomography,” Frontiers in Neuroscience, 10:543, 2016.


Y. Li, J. Qin, W. Liu and S. Osher, “Graph Fractional-Order Total Variation EEG Source Reconstruction,” 38th Annual International Conference of the IEEE Engineering in Medicine and Biology Society (EMBC), pages 101104, Orlando, Florida, August 2016.


Z. Peng, T. Wu, Y. Xu, M. Yan, and W. Yin. “Coordinate friendly structures, algorithms and applications,” Annals of Mathematical Sciences and Applications, 1:57-119, 2016.


T. Pock and A. Chambolle. “Diagonal preconditioning for first order primal-dual algorithms in convex optimization,” 2011 International Conference on Computer Vision, pages 17621769. IEEE, 2011.

THANK YOU!!!

Email: jing.qin@montana.edu